Electrochimica Acta 290 (2018) 556–567

Contents lists available at ScienceDirect

Electrochimica Acta

journal homepage: www.elsevier.com/locate/electacta

Experimental and theoretical insights into the electrooxidation pathway of azo-colorants on glassy carbon electrode

Paulina Sierra-Rosales [a, *], Cristhian Berríos [b], Sebastián Miranda-Rojas [c, **], Juan A. Squella [d]

[a] Programa Institucional de Fomento a la Investigación, Desarrollo e Innovación, Universidad Tecnológica Metropolitana, Ignacio Valdivieso 2409, P.O Box 8940577, San Joaquín, Santiago, Chile
[b] Laboratorio de Electrocatálisis, Departamento de Ciencias del Ambiente, Facultad de Química y Biología, Universidad de Santiago de Chile, Santiago, Chile
[c] Departamento de Ciencias Químicas, Facultad de Ciencias Exactas, Universidad Andres Bello, República 275, Santiago, Chile
[d] Departamento de Química Orgánica y Fisicoquímica, Facultad de Ciencias Químicas y Farmacéuticas, Universidad de Chile, 8380492, Santiago, Chile

ARTICLE INFO

Article history:
Received 24 May 2018
Received in revised form
20 July 2018
Accepted 13 September 2018
Available online 17 September 2018

Keywords:
Sunset yellow
Ponceau 4R
Allura red
Colorants electrooxidation
Density functional theory

ABSTRACT

Sunset yellow, Allura red and Ponceau 4R are azo-colorants with similar chemical structures. These colorants were studied by electrochemical methods at a glassy carbon electrode in phosphate buffer solution (pH 7.0), combined with UV–Vis spectroscopic and theoretical methods to unveil their electrooxidation pathway. The electrooxidation of the azo-colorants showed an irreversible process for allura red and an electrochemical/chemical process for sunset yellow and ponceau 4R. The experimental potentials and the number of electrons involved in the oxidation process were correlated with those obtained from theoretical studies to support our findings. The characteristic bands of each colorant experimentally observed by UV–Vis were successfully assigned to specific molecular orbital transitions by theoretical calculations. According to this, the band close to 450 nm was assigned to electronic transitions centered in the azo-moiety, where spectroelectrochemical studies showed its disappearance after oxidation of the colorants. These results exposed that the azo-moiety is chemically affected by the oxidation process. The resonance structures of the colorants oxidized through the azo-moiety were confirmed by spin density analysis, suggesting the azo group as the electroactive center towards the oxidation of these colorants. In this article, we used a combined experimental and theoretical approach to provide new insights into the controversial aspects of the electrochemical oxidation of sunset yellow, allura red and ponceau 4R. As a consequence of these results, we propose a new reaction pathway involving the direct oxidation of the azo group.

1. Introduction

Food colorants are added to food products to improve their aesthetic appeal to the consumers. The synthetic colorants are employed by food industry mainly due to their stability and cost of production compared to natural colorants. They are classified into five categories: azo compounds, the dye containing the triarylmethane group, quinoline yellow (chinophthalon derivatives), xanthenes (erythrosine) and indigo dye [1].

Sunset yellow FCF (SY), allura red AC (AR) and ponceau 4R (P4) are synthetic water-soluble azo compounds. In their structure they contain one azo group (-N=N-) as chromophore in association with aromatic structures with functional groups such as −OH and $-SO_3^-$ (Fig. 1). Azo-compounds are electroactive molecules and can be involved in both oxidation and reduction reactions [2,3].

The electrochemical reduction of the azo group has been widely studied and its reduction mechanism is well known [3,4]. The main concern about azo compounds is that their reduction products form aromatic amines, which are associated with health issues and carcinogenicity [3,5–7].

On the other hand, the electrooxidation of these azo colorants has been attributed to the −OH group [8–10]. This mechanism has been used by several authors to explain the electrooxidation of azo-dyes, even though in some cases the number of protons and electrons involved is different. This exposes the absence of a detailed

* Corresponding author.
** Corresponding author.
E-mail addresses: psierra@utem.cl (P. Sierra-Rosales), sebastian.miranda@unab.cl (S. Miranda-Rojas).

https://doi.org/10.1016/j.electacta.2018.09.090
0013-4686/

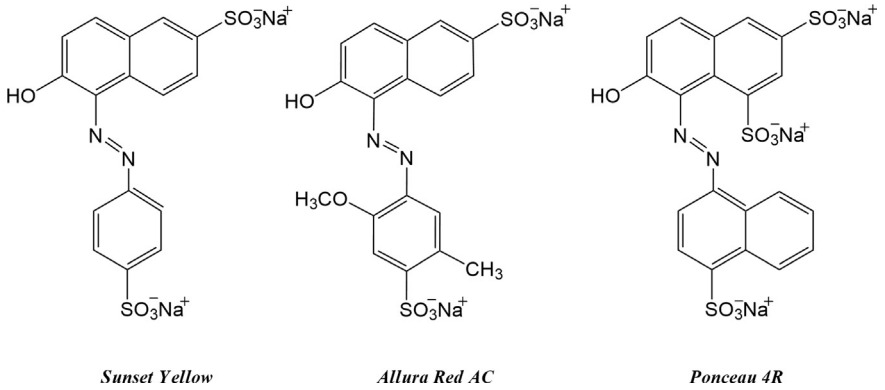

Fig. 1. Chemical structures of sunset yellow (SY), allura red AC (AR) and ponceau 4R (P4).

reaction mechanism, where in all cases the mechanism is based on the electrochemical response of the phenolic group instead of the aryl-azo group in the oxidation process [2,11]. In fact, Gooding et al. [3] indicates that in solid electrodes as glassy carbon, the azo bond is more easily oxidized than reduced. Additional evidence suggesting the azo moiety as the redox active region of dyes comes from the study of the electrochemical behavior of the azo dye methyl orange (MO), which does not have hydroxyl groups. Therefore, the oxidation of MO resulted in its polymerization through the azo group on the electrode surface [12].

In this article we combined theoretical and experimental data to provide new insights about the electrooxidation mechanism of SY, AR and P4 colorants and a new reaction pathway is proposed involving the azo group supported by experimental evidence.

2. Experimental

2.1. Reagents

SY (CAS 2783-94-0), AR (CAS 25956-17-6) and P4 (CAS 2611-82-7) were of analytical standard grade (≥95%), purchased from Sigma-Aldrich and dissolved in water to prepare a 0.5 mM stock solution. The sample solutions were prepared by diluting the stock solution with buffer. For the pH study, a 0.1 M Britton-Robinson buffer was used (boric acid, phosphoric acid and acetic acid). The other experiments were performed in phosphate-buffered saline (0.1 M PBS, pH 7.0) as the supporting electrolyte solution. All the solutions were prepared with ultrapure water from a Millipore Milli-Q System.

2.2. Instruments

Cyclic voltammetry (CV) and differential pulse voltammetry (DPV) were performed with a potentiostat CHI 650E (CH Instruments Inc., USA). A conventional three-electrode system was used with a glassy carbon electrode (GCE) (Model CHI 104, CH Instruments Inc., USA), a platinum wire as the counter electrode (BASiMW-1032) and Ag/AgCl (3 M NaCl) (Model RE-5B, BAS) as the reference electrode. All potentials are given relative to the reference electrode. A magnetic stirrer provided convective transport when necessary. The working electrode was polished with 0.30 and 0.05 μm alumina slurries for 1 min before use.

The UV–visible spectra were recorded in the 190–800 nm range by using a UNICAM UV-3 spectrophotometer with diode array. Acquisition and data treatment were performed with Vision 2.11 software.

2.3. Electrochemical measurements

Electrochemical measurements of SY, AR and P4 were carried out in 0.1 M PBS at pH 7.0. Cyclic voltammograms (CV) and differential pulse voltammograms (DPV) were performed over the potential range of 0.0 V–1.2 V, and the oxidation peak currents were recorded. The DPV operating conditions were a potential increment of 0.004 V, pulse amplitude of 0.05 V, and pulse period of 0.2 s. All experiments were conducted at room temperature and in quadruplicate.

2.4. Controlled-potential electrolysis (CPE) experiments

Controlled-potential electrolysis (CPE) was performed on a reticulated porous carbon electrode to oxidize the colorants in 0.1 M PBS pH 7.0 as supporting electrolyte. A three-electrode circuit system with an Ag/AgCl electrode was used as reference and a Pt wire as a counter electrode. The potential applied to oxidize each colorant was +0.8 V (SY and P4) and +0.9 V (AR). These values are at least 100 mV higher than the oxidation potential of each colorant, with which we ensure the complete oxidation during the electrolysis. A CHI 650E assembly was used to electrolyze the different colorants. The electrolyzed solutions were analyzed by UV–vis experiments to follow the electrolysis in-situ.

2.5. Computational methods

2.5.1. Oxidation potentials

To aim towards the highest accuracy possible at computationally modeling the oxidation potentials using the DFT level of theory, we performed a systematic study using ten different density functionals searching the most appropriate for these systems. The list includes the M062X [13], M06L [14], M11 [15], M11-L [16], BHandHLYP [17], PBE [18], PBE0 [19], revPBE [20], BP86 [21,22] and B3LYP [23,24]. In addition, we used the 6-311 + g(d,p) basis set [25], a triple-ζ basis set with polarization functions able to provide an acceptable accuracy for the energetics. Diffuse functions were added to properly describe the anionic nature of these systems. At each level of theory defined by the functional, we performed a full geometry optimization of the systems. To calculate the oxidation potentials we used the following equation:

$$E_{ox} = -\left(\frac{-\Delta G^{\circ}_{ox}}{nF} + SHE\right) \quad (1)$$

where E_{ox} corresponds to the oxidation potential, ΔG°_{ox} to the free energy of the oxidation reaction, n is the number of electrons

involved, F is the Faraday constant (96485 C mol^{-1}) and SHE is the potential of the standard hydrogen electrode (4.28 V) [26]. Therefore, the problem is reduced to calculate ΔG°_{ox} of the oxidation reaction:

$$R_s \rightleftharpoons O_s + n\bar{e}_g \quad (2)$$

Here, R refers to the reduced species, namely the colorant, and O refers to the oxidized colorant. Notice that one of the species should be charged to keep the neutrality of the balanced equation. The subscripts indicate if the species is in solution (s) or gas phase (g). To obtain ΔG°_{ox}, the thermodynamic cycle shown in Scheme 1 was used, according to which we can calculate ΔG°_{ox} from the sum of the gas-phase adiabatic ionization energy (IE_g) and the difference in free energy of solvation between the oxidized and reduced species ($\Delta\Delta G_{solv}$) (Eqs. (3) and (4)).

$$\Delta G^{\circ}_{ox} = IE_g + \Delta\Delta G_{solv} \quad (3)$$

$$\Delta\Delta G_{solv} = \Delta G^{*}_{s,O} - \Delta G^{*}_{s,R} \quad (4)$$

where $\Delta G^{*}_{s,R}$ and $\Delta G^{*}_{s,O}$ are the free energy of solvation of the reduced and the oxidized species, meaning the free energy change from taking the specie from the gas-phase to the aqueous-phase. These free energies were obtained by zero-point energy correction and thermal correction at 298.15 K, where solvation was incorporated through the SMD solvation model [27]. The free energy used for the electron was the obtained with the Fermi-Dirac statistics at 298 K (0.752 kcal mol^{-1}). For further details regarding the methodology refer to the thorough work carried out by Arey et al. [28]. All calculations here performed were carried out by using the Gaussian 09 suite of programs [29]. Finally, the E_{ox} values were converted from SHE to Ag/AgCl (3M) reference electrode by subtracting 0.209 V to the calculated values [30].

2.5.2. UV–visible spectra calculation

An exhaustive computational study carried out by Adamo et al. [31] defined the functionals best suited to describe the main spectral features of some types of colorants, among which the azo-compounds were included. Among the studied functionals, PBE and PBE0 showed an outstanding performance, both functionals included in our set under study. However, only PBE0 showed a good behavior at describing the oxidation potentials according to our calculations, therefore PBE0 was selected for the excitation energy calculations to keep consistency. The same basis set as for the energy calculations was implemented (6-311 + g(d,p)). The excitation energies were obtained by the time-dependent perturbation theory approach (TD-DFT) [32,33] based on the random-phase approximation (RPA). UV–visible spectra calculations were performed considering the environment effect by using the same implicit solvation model used for the oxidation potentials determination (SMD). Each calculation involved the estimation of 100 singlet excitation states. For each selected singlet excitation, we considered for the analysis those molecular orbital transitions with contributions larger than 20%. Due to the delocalized nature of molecular orbitals, in order to obtain chemical insights from these, we determined the molecular orbital decomposition following the natural atomic orbital (NAO) approach. For this purpose, we calculated the NAOs with the NBO program [34] implemented in Gaussian 09 and performed the analysis by using the Multiwfn v3.5 program [35].

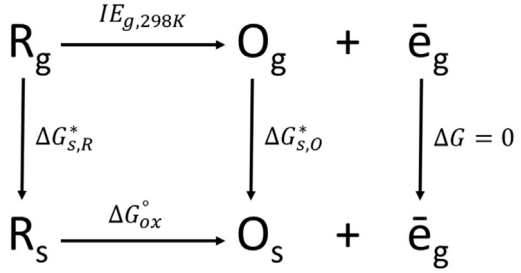

Scheme 1. Thermodynamic cycle used to calculate the Gibbs free energy of the oxidation reaction (ΔG°_{ox}). $IE_{g,298K}$ corresponds to the gas-phase adiabatic ionization energy calculated at 298 K. $\Delta G^{*}_{s,X}$ (X = R,O) are the Gibbs free energies of solvation of the reduced and oxidized states, respectively (Adapted from Ref. [28]).

3. Results and discussion

3.1. Electrochemical oxidation

General information about the redox behavior of AR, SY and P4 was obtained by cyclic voltammetry in 0.1 M PBS (pH 7.0) on a bare glassy carbon electrode (GCE). The cyclic voltammograms of 0.5 mM of the colorants at a scan rate of 50 mV s^{-1} are shown in Fig. 2. All colorants showed a single oxidation peak between 0.5 and 1.0 V. On the reverse scan, at 50 mV s^{-1} no reduction peak was detected for AR and SY. For P4, an anodic peak (+0.7 V) and a small cathodic peak (+0.5 V) was observed.

The influence of the scan rate on the peak currents and potentials of AR, SY and P4 was studied by increasing it from 0.05 to 1.0 V s^{-1} (Fig. 3). A diffusion-controlled process for the three colorants was observed by a linear relationship between i vs. $\nu^{1/2}$ and the slope of ln i versus ln ν plot, which was close to 0.5 (not shown). For AR a single anodic peak was observed (Fig. 3A). The oxidation peak potential ($E_{p,a}$) is gradually shifted to more negative potentials with the scan rate, confirming the irreversibility of the process. To determine the number of electrons involved in the oxidation process of AR, we use an equation that relates the $E_{p,a}$ with the scan rate as follows [36]:

$$E_p = E^{\theta'} - \frac{RT}{\alpha nF}\left[0.780 + ln\left(\frac{D^{1/2}}{k^0}\right) + ln\left(\frac{\alpha nF\upsilon}{RT}\right)^{1/2}\right] \quad (5)$$

$$E_p = K + \frac{RT}{2\alpha nF}\ln \upsilon \quad (6)$$

where $E^{\theta'}$ is the formal potential; D is the diffusion coefficient; k^0 is the standard heterogeneous rate constant; F is the Faraday constant; α is the transfer coefficient; n is the number of electrons involved in the process; R and T represent their usual meaning. According to equation (6), the plot of E_p vs ln ν showed a linear relationship (R = 0.992), where the slope obtained was of 26 mV (Fig. 3B). The value of the slope equals to $RT/2\alpha nF$, which results in $\alpha n = 0.49$. For a totally irreversible system, it is assumed that $\alpha = 0.5$; therefore, we obtained that one electron is transferred in the oxidation of AR.

In the case of SY, at low scan rates (50 and 100 mV s^{-1}) only an anodic peak was observed (Fig. 3C). When the scan rate increased up to 100 mV s^{-1} a cathodic peak appeared. This is indicative of a chemical process following the electron transfer step [36,37], where the chemical reaction is fast which rapidly remove the oxidized specie from the region near to the electrode surface. Therefore, no reverse peak was observed at low scan rates. When the scan rate is increased, the cathodic peak increases indicating that the electron transfer step is reversible and is followed by an irreversible chemical step (E_rC_i):

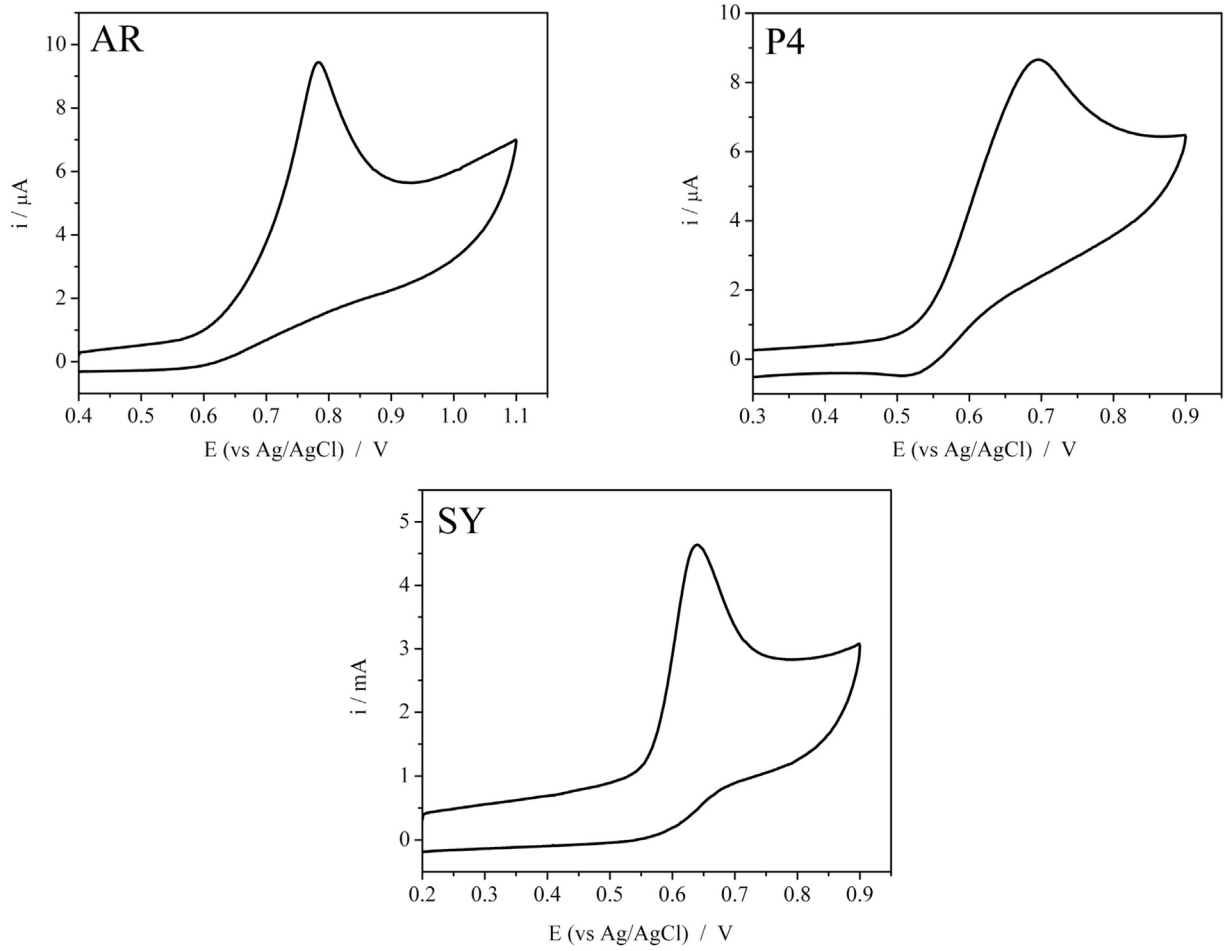

Fig. 2. Cyclic voltammograms of 0.5 mM of the colorants in 0.1 M PBS at pH 7.0. Scan rate = 50 mV s^{-1}.

$$R \rightleftharpoons O + n\bar{e}$$

$$R \rightarrow Y \quad (7)$$

As a diagnostic test for EC reactions, the chemical reaction is of first order when in a E_p *vs* ln ν plot the shifting in the anodic peak potential is $30/n$ mV in the pure kinetic zone [37]. In our case the slope value was equal to 15 mV indicating that for SY $n = 2$ (Fig. 3D). Another diagnostic test for EC reactions is when the $i_{p,c}/i_{p,a}$ ratio is less than one but it increases with the scan rate until it get values close to the unity, which was confirmed for SY. After plotting $E_{p,a}$ *vs* the logarithm of the concentration of SY (log C_{sy}) (not shown), we obtained a zero slope which confirms that the oxidation of SY involved an irreversible first-order chemical process (E_rC_i) [38].

For P4, one anodic peak (+0.7 V) and a small cathodic peak (+0.55 V) in the reverse scan were observed (Fig. 3E). The initial value of ΔE_p (~190 mV) increases with the scan rate, reaching a final value of ~430 mV at the highest scan rate. The systems cannot be considered as reversible due to the high ΔE_p and the differences in currents. Similarly to SY, the cathodic current peak of P4 increases with the scan rate but the $i_{p,c}/i_{p,a}$ ratio did not reach the unity. Also, this was confirmed by plotting $E_{p,a}$ *vs* the logarithm of the concentration of P4 (log C_{P4}). Therefore, an E_rC_i mechanism is proposed for P4. After plotting E_p *vs* ln ν (Fig. 3F), we observed that the anodic potential shifts with the scan rate with a slope of 28 mV, with which we calculated an $n = 1.1$. The parameters obtained are summarized in Table 1.

Computational chemistry methods were carried out for the electrooxidation process to obtain deeper insights about the electron transfer process. The first step was to explore the nature of the electron transfer of one electron. After performing an exhaustive exploration through several levels of theory (Tables S–1), the results with best agreement with the experimental data were obtained with the BP86 density functional (Table 2). These results show an excellent agreement with the experimental data, with deviations of −0.04 V and −0.01 V for P4 and AR. On the other hand, the deviation of the first electron potential of SY with respect to the experimental result confirms that this is not a 1-electron process. The experimental oxidation potential of SY is lower than the other two colorants, showing the opposite trend when compared to the calculations. The experimental results showed that the oxidation pathway of SY involves a 2-electron process. However, it is expected that the second electron potential to be higher than the first, confirmed by the 0.92 V calculated for SY. At this point, one proposal was that the second electron transfer was preceded by a proton release from the −OH group that may decrease the oxidation potential. After calculating this oxidation potential, it decreased to 0.43 V, which despite of the deviation from the 0.64 V experimentally obtained, is the only pathway leading to a lower oxidation potential for SY with respect to the other two colorants. Thereby, while P4 and AR involve a 1-electron oxidation process, SY involves 2-electrons and one proton in the first part of the mechanism, where the proton is released after the first electron transfer.

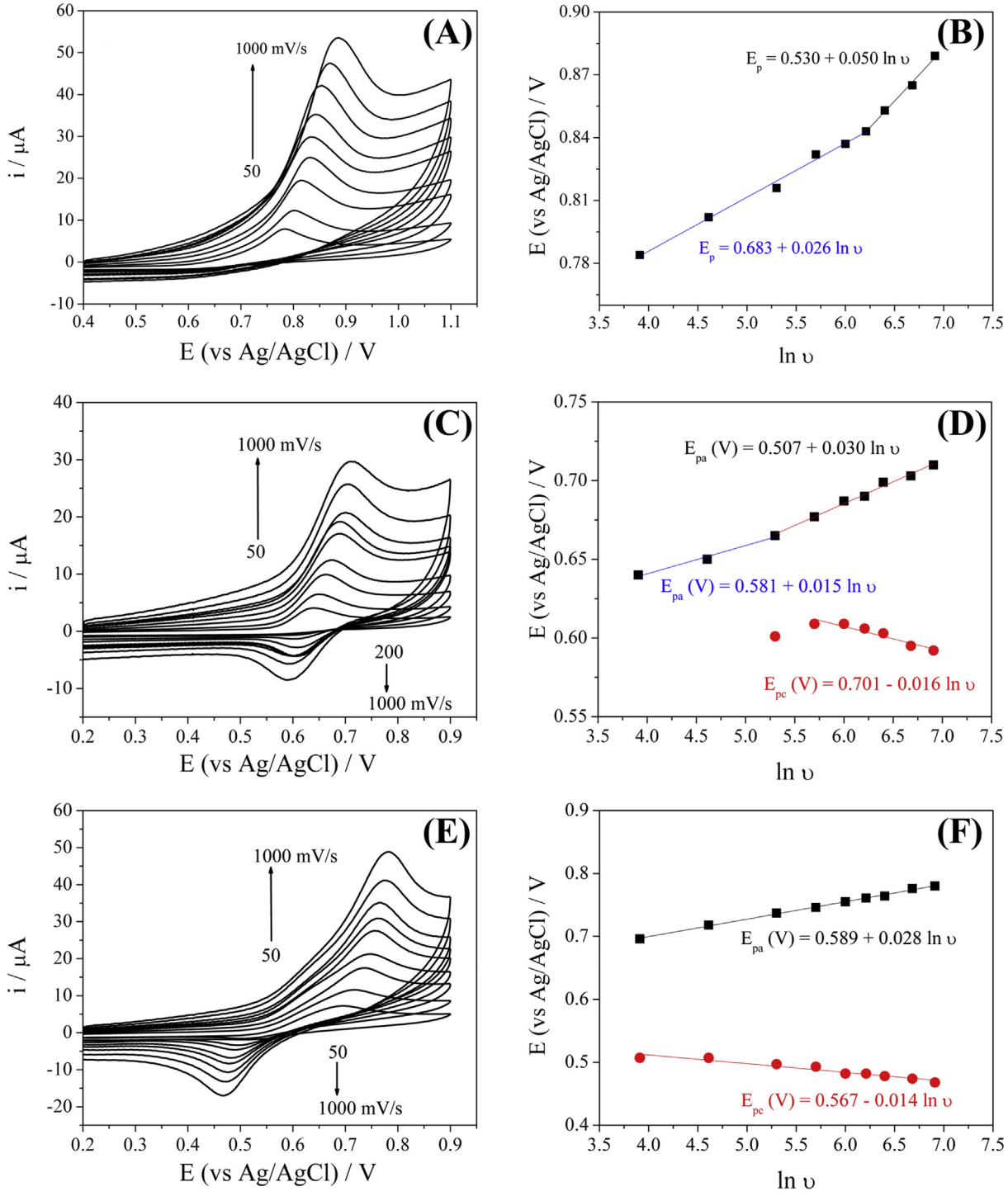

Fig. 3. Cyclic voltammograms of 0.5 mM solutions of the colorants in 0.1 M PBS at pH 7.0 at various scan rates: 50, 100, 200, 300, 400, 500, 600, 800 and 1000 V s^{-1}, respectively. (A–B) AR, (C–D) SY and (E–F) P4.

Table 1
Summary of parameters of 0.5 mM AR, SY and P4 in 0.1 M PBS, pH 7.0 obtained by cyclic voltammetry.

Colorant	E_p (V) vs Ag/AgCl 3 M	∂ln i/∂ln ν	Redox process	$\partial E_p/\partial \ln \nu$	N° electrons
AR	0.76	0.47	Ei	30	0.98
SY	0.64	0.54	E_rC_i	15	1.8
P4	0.68	0.41	E_rC_i	30	1.1

Table 2
Experimental data and theoretical calculation of the oxidation potential of colorants.

Colorant	Experimental E_p/V	Theoretical E_p/V		
		BP86 (1e)[a]	BP86 (2e)[b]	BP86 (1e/1H$^+$,1e)[c]
AR	0.76	0.75	–	–
P4	0.68	0.64	–	–
SY	0.64	0.88	0.92	0.43

[a] E_p obtained after one electron transfer.
[b] E_p obtained after two electron transfer of SY.
[c] E_p obtained after the second electron transfer of SY preceded by a proton released.

To rationalize the differences on the oxidation potentials between the colorants studied, we explored the relationship between the chemical structures and the variations on the potentials. According to Table 2, the 1-electron potentials follow the trend SY (0.88 V, for the first e-transfer) > AR (0.76 V) > P4 (0.68 V), where for SY it was obtained through computational methods. Interestingly, SY, AR and P4 can be considered as functionalized forms of Sudan I because of its chemical structure, which only has the hydroxyl group (Fig. S-1). Setting the potential of Sudan I as a base allows to explain the differences between the colorants here studied by analyzing the effect that the functional groups (electron-withdrawing (EW) or electron-donating (ED)) have on Sudan I. In principle, EW groups increased the oxidation potentials; whereas ED groups decrease it, as it was observed by Ungureanu et al. for azo-azulene compounds [2]. Sudan I has an anodic peak at 0.72 V on GCE (PBS, pH 7.0) [39]. SY has the same chemical structure of Sudan I but with two sulfonate groups (one in the naphthol ring, and the second in the benzyl ring). Then, as expected from the effect of EW groups as sulfonate, the potential is increased when compared to Sudan I from 0.72 V to 0.88 V. The addition of ED groups to SY such as $-OCH_3$ and $-CH_3$ leads to the structure of AR, functional groups that should decrease the oxidation potential with respect to SY. As expected, the potential decreased from 0.88 V to 0.76 V. On the other hand, the incorporation of a naphtyl group to SY leads to the structure of P4, which is an ED group. This chemical modification induces a decrease in the oxidation potential from 0.88 V to 0.68 V. Additionally, P4 has an extra sulfonate group when compared to SY, but the presence of this group in the naphthol moiety did not increase the potential and we suggest that the effect of the ED group was dominant. To complete our analyses we considered the oxidation potential of the dye Amaranth, which has two sulfonate groups in the naphthol ring, but in different positions compared to P4. In the case of Amaranth, the sulfonate group is next to the –OH and it affects the oxidation potential of the molecule increasing the potential to 0.75 V [40]. In all the cases, the presence of different functional groups in the naphthol ring played a less important role in the anodic potential probably due to the distance of the groups with the aryl-azo moiety.

In order to determine if the colorants were adsorbed onto the electrode surface after their oxidization, we performed consecutive cyclic voltammograms of 0.5 mM of AR, SY and P4 in 0.1 M PBS at pH 7.0 (at $\nu = 50$ mV s^{-1}) (Fig. S-2). No reduction peak was observed in the reverse scan for the three colorants, which indicates that the oxidation products are not electroactive. During successive scans, the height of the oxidation peaks decreases (34% for P4, 26% for SY and 10% for AR) and a positive shift in potential is observed, which could be explained by two processes: (1) the generation of a non-electroactive specie with the adsorption of this product onto the electrode surface or (2) the polymerization of the oxidation product onto the electrode surface. In the case of 2-naphthol or chlorinated phenols onto GCE, the decrease in electroactivity is attributed to the formation of a polymeric film due to the oxidation of the –OH groups [41–43]. But, for azo dyes like methyl orange (MO), which lacks –OH groups in its structure and it is chemically similar to the azo dyes studied here, the decrease in electroactivity was attributed to the deposition of aromatic polymeric products on the electrode surface after oxidation of the azo group [12]. Therefore, in order to clarify the possible products of the oxidation mechanism, it is necessary to determine whether the redox center of the azo colorants is derived from the hydroxyl group or from the azo moiety.

In addition, we studied the pH dependence of the anodic peak of the colorants over a wide pH range (2.0 and 13.0), using differential pulse voltammetry (DPV) in 0.1 M Britton-Robinson buffer solution. As shown in Fig. 4, the peak potentials (E_p) linearly shifted to more negative values with pH range up to a certain value depending on the colorant (pH 11.0 for SY and P4; pH 13 for AR). In the linear range, the absolute values of the slopes were similar for all the colorants (32, 36 and 39 mV per pH unit for P4, AR and SY, respectively). Different authors have associated slopes values close to 40 mV per pH unit with probable dimerization of the molecules, leading to an irreversible product adsorption [44–46]. This is in agreement with the results obtained with consecutive cyclic voltammograms in the previous section. For all colorants, the oxidation mechanism at GCE is pH-dependent and protons are involved.

Following the approach used by Barrientos et al. [47], we estimated the voltammetric pK_a values from the breaks in the graphs E_p vs. pH. According to this, the pK_a values of SY and P4 were of 11.5 and 12.0; respectively. In the case of AR, no break was observed, therefore, the pK_a value apparently is close to 13 and the break is not perceptible at the studied pH range. Next, we analyzed DP voltammograms for the colorants (see Fig. S-3) from which it is possible to appreciate changes in the DPV profiles at pH values close to the estimated voltammetric pK_a values. For SY (Fig. S-3 (A,B)), the change in the DPV profile was noticed between pH 10.0–11.0, where the current of the peak located close to 0.6 V decreases with the pH and a second small peak close to 0.9 V started to appear. In the case of P4 (Fig. S-3 (C, D)), the DPV profiles at higher pH values (11.0, 12.0 and 13.0), showed a significant decrease in current and a second peak close to 0.6 V is noticed. Again, these changes are present at pH values close to the calculated pK_a of P4. Finally, for AR (Fig. S-3 (E, F)), a small change in the DPV profile appears at pH 13.0, where a decrease in current was observed. This confirmed that the voltammetric pK_a for AR could be close to pH 13, in agreement of the results present in Fig. 4.

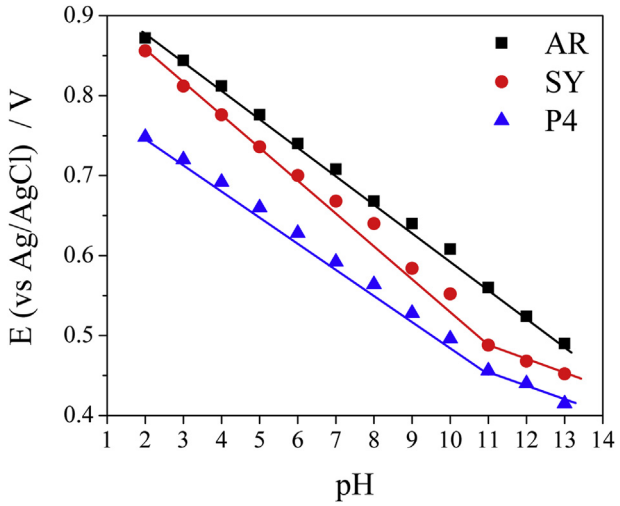

Fig. 4. Effect of pH on the anodic peak potential of 10 μM of AR, P4 and SY in 0.1 M Britton-Robinson buffer solution.

3.2. UV–visible spectroscopic studies

The UV–visible absorption spectra of the colorants in 0.1 M PBS at pH 7.0 are shown in Fig. 5. AR and SY exhibit three main absorption peaks with maxima absorbance around 234, 315 and 490 nm. For P4, the same bands are observed but with a slight bathochromic shift. The absorption band at around 490 nm is directly related to the color of the solution and the peak at about 315 nm has been related to the aromatic rings [12,48]. These maximum absorption peaks are similar to the observed for other azo dyes with similar structure [12,49–52]. Ahmad et al. [49] studied SY, where they assigned the band at 481 nm to an intramolecular charge transfer (ICT) without providing details about the groups involved in this ICT. In the case of the azo dye methyl orange (MO), the maximum wavelength observed at 506 nm was assigned by Ramirez et al. [53] to a π-π* of the conjugated chromophore system composed of two benzenic rings and one azo group (chemically similar to SY). Wang et al. [52] followed the UV–vis of carmoisine (or acid red 14, E122). This azo-colorant showed a well-resolved band at 514 nm what was assigned to the n-π* transition of –N=N- group. Despite that what has been reported by these authors agree in terms of the main bands that seems to be the main

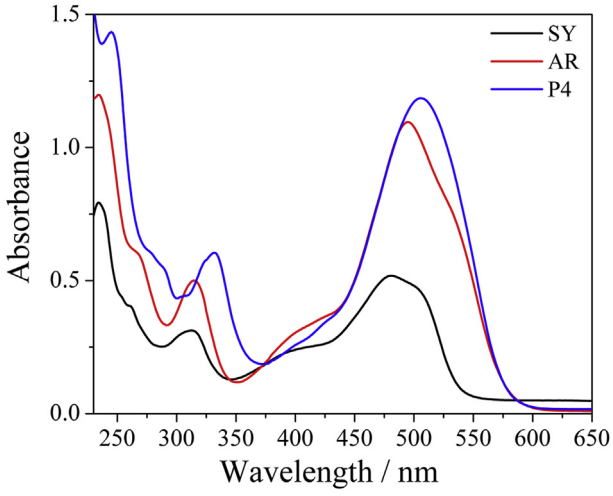

Fig. 5. UV–Vis of 50 uM SY, AR and P4 in 0.1 M PBS at pH 7.0.

electronic spectra feature for these colorants, there are several discrepancies regarding the bands assignments. In order to shed light into the electronic transitions nature, we performed computational calculations of the electronic spectra to properly assign the bands and compare with the colorants here studied AR, SY and P4.

In Table 3, the calculated electronic excitations (λ_{calc}) reproduce the three main bands of the UV–visible spectra of each colorant (λ_{exp}). The molecular orbitals involved in each electronic transition of SY are shown in Fig. 6, which were used to define the nature of the transition and the main regions of the molecule involved in each transition. For AR and P4 the molecular orbitals are shown in the supporting information (Fig. S-4).

According to our results, the most important spectral feature for the azo-colorants here studied corresponds to the band around 490 nm. This is the only band that is properly described by one electronic excitation, whose contribution is largely dominated by the HOMO-LUMO transition (>81%). Its relevance rises from the fact that this excitation involves an n-π* transition, where the HOMO orbital is partially dominated by one of the lone pairs located in the azo-moiety. It also contains some contribution from a π-bonding orbital located in one of the aromatic rings, but it is only a minor contribution. The LUMO on the other hand, is highly dominated by a π* contribution located in the azo-moiety. Therefore, the presence of this band could be used to evidence the structural integrity of the azo-moiety. The band around 315 nm corresponds to a π-π* transition. This transition involves electrons from both aromatic rings with some predominance of the naphthol group, towards a π* orbital mostly located at the azo moiety. Similar to the band at 490 nm, this band will evidence the structural integrity of the azo moiety as it is involved in the electronic transition. Finally, the band around 234 nm on the other hand is a π-π* transition that only involves the aromatic rings, therefore is should be the less affected after structural modifications to the azo-moiety.

Additionally, in order to determine experimentally the dissociation constants of the colorants in water we followed the influence of pH on the UV–vis spectra. The analysis of the data was done following three methods, and the final pK_a values were obtained as an average value between methods [54,55]. Those values are summarized in Table 4. As can be seen, in aqueous solution the pK_a values are close to the estimated voltammetric pK_a values obtained from the breaks in the graphs E_p versus pH (Fig. 4).

Finally, controlled-potential electrolysis on reticulated carbon

Table 3
Calculated electronic excitations of the UV–visible spectra of each colorant.

Colorant	λ_{exp} (nm)	λ_{calc} (nm)	Contributions	f[a]	Transition type
SY	234	240.05	103 → 107 (30.7%)	0.3234	[π-naphthol + n-azo] → [π*-naphthol]
		219.84	104 → 109 (24.2%)	0.2619	[π-naphthol + n-azo] → [π*-benzyl]
	313	327.34	103 → 106 (52.7%)	0.0359	[π-naphthol + n-azo] → [π*-azo]
		308.29	104 → 106 (41.4%)	0.0904	[π-naphthol + n-azo] → [π*-azo]
		292.99	105 → 107 (74.7%)	0.1666	[π-naphthol + n-azo] → [π*-naphthol]
			100 → 106 (70.0%)		[π-benzyl + n-azo] → [π*-azo]
	481	492.67	105 → 106 (81.2%)	0.0726	[n-azo + π-naphthol] → [π*-azo]
AR	234	236.77	116 → 120 (31.5%)	0.5013	[π-benzyl] → [π*-naphthol]
			116 → 121 (24.6%)		[π-benzyl] → [π*-azo + π*-benzyl]
	315	356.13	114 → 118 (54.7%)	0.1192	[π-naphthol/benzyl/azo] → [π*-azo]
		324.56	115 → 118 (77.4%)	0.0322	[π-naphthol] → [π*-azo]
		307.99	117 → 119 (81.8%)	0.0458	[n-azo + π-naphthol] → [π*-naphthol]
	495	493.46	117 → 118 (83.4%)	0.0938	[n-azo + π-naphthol] → [π*-azo]
P4	245	219.06	135 → 142 (42.4%)	0.3470	[π-naphthol] + π-azo] → [π*-naphthol]
	332	367.24	137 → 139 (87.6%)	0.1357	[π-naphthyl][b] → [π*-azo]
		331.14	138 → 140 (82.7%)	0.0756	[n-azo + π-naphthol] → [π*-naphthol]
	506	539.63	138 → 139 (84.6%)	0.0774	[n-azo + π-naphthol] → [π*-azo]

[a] Oscillator strength.
[b] P4 has a naphthyl and a naphthol group connected by the azo moiety and both aromatic systems are involved in the transitions calculated.

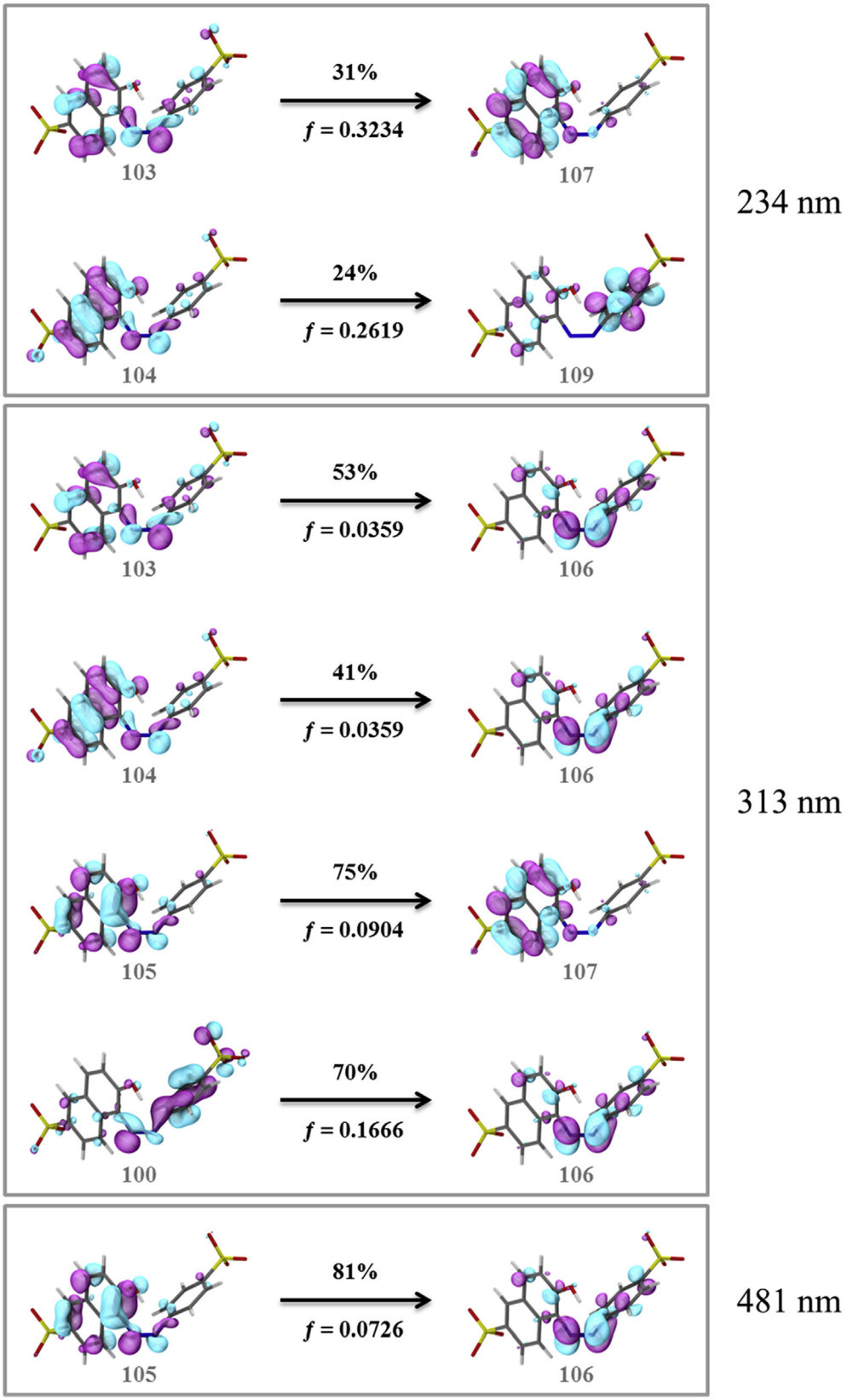

Fig. 6. Active molecular orbitals in the electronic transition of SY.

Table 4
Comparison of the pK_a data obtained by UV–visible spectroscopy.

Colorant	pK_a (method 1)[a]	pK_a (method 2)[a]	pK_a (method 3)[b]	Average
AR	12.3	12.2	11.5	12.0 ± 0.44
SY	11.0	10.3	10.3	10.5 ± 0.40
P4	11.8	11.0	11.1	11.3 ± 0.44

[a] Ref. [51].
[b] Ref. [52].

electrode was carried out in 0.1 M PBS (pH 7.0) and the spectra changes on the UV–vis during 60 min were recorded. The application of an oxidation potential of +0.9 V for AR and +0.8 V for SY and P4, produces a decrease in the absorption of the original bands with electrolysis time indicating that the compounds concentration is decreasing to give products. For SY and AR (Fig. 7A–B) the intensities of the bands around 315 and 490 nm decrease during electrolysis until total disappearance. For these two colorants, a total discoloration of the solution is obtained after 10 and 25 min, respectively. The disappearance of the bands that are responsible of the color of the solution is caused by the modification of the electronic structure of the orbitals involved in these electronic transitions. According to our theoretical results, the main centers in which these orbitals are located is the azo group. Then, the loss of these bands point out a modification of this group that could cause the displacement of the band outside of the studied range, or if it is a dissociation of the azo moiety, the loss of this transition. Both scenarios allow to explain the relationship of the loss of color with

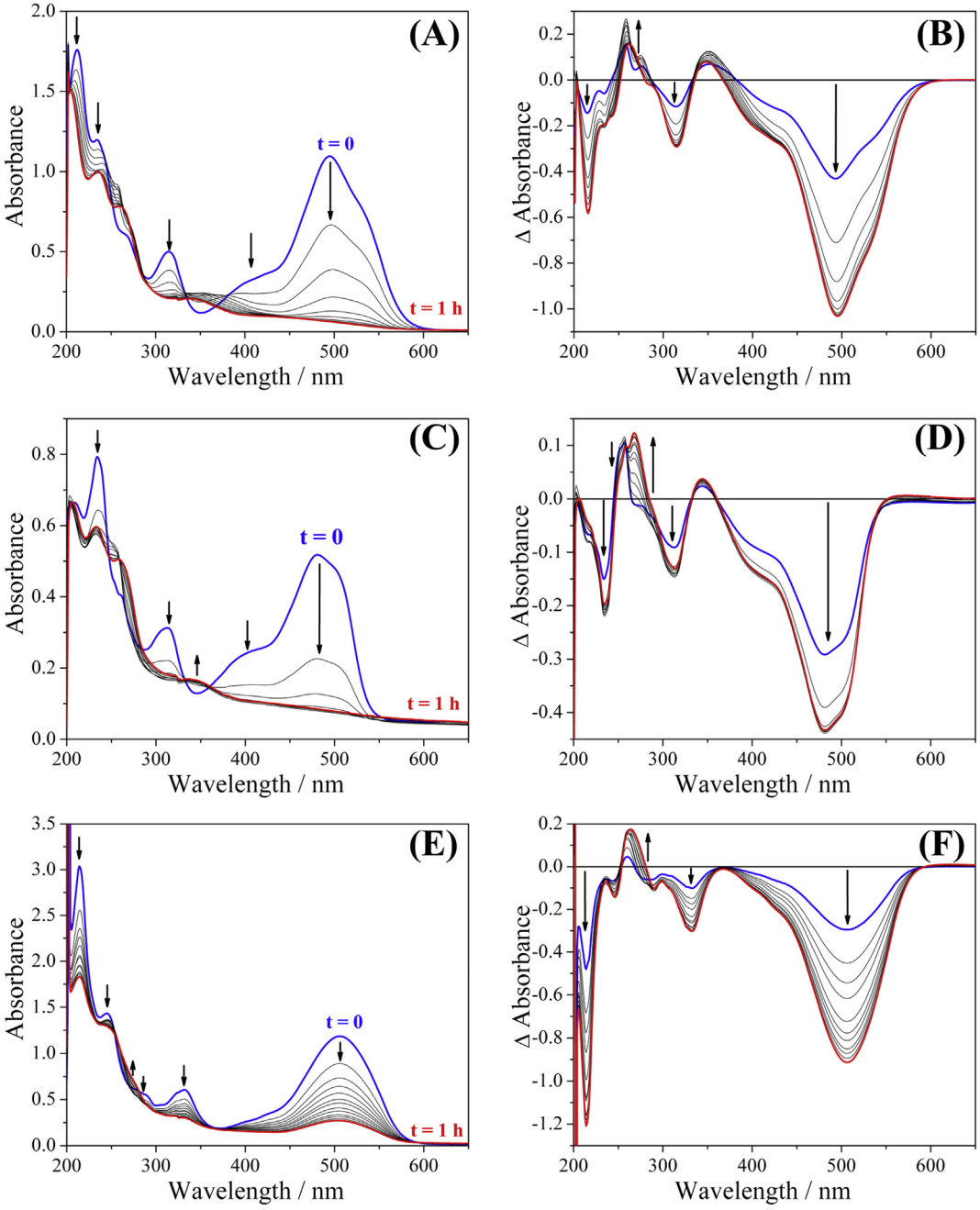

Fig. 7. UV–Visible changes and Differential UV–Visible spectra of 50 uM of colorants during 1 h of electrolysis. (A–B) AR, (C–D) SY and (E–F) P4, respectively. Electrolysis potential: +0.9 V (AR) and +0.8 V (P4 and SY). Electrolysis medium: 0.1 M PBS at pH 7.0.

the oxidation of the azo group. After the oxidation, the experimental spectra of the molecule only show transitions from the aromatic ring scaffolds, as supported by our theoretical studies, transitions that are outside of the visible range. Therefore, the combination of our theoretical and experimental results shows that the oxidation process of the colorants deactivates the azo bond in a short time. In the case of P4 (Fig. 7C), after 60 min of electrolysis the bands decrease in intensity but the solution was not totally translucent as SY and AR. In all the cases, the most affected group in the chemical structure of the colorants is the azo bond indicating that it is the most active group for oxidation. This is in agreement with the spectral changes observed for other azo dyes [56,57].

With the differential UV–Visible spectra the appearance of new bands was noted (Fig. 7D–F). In the case of SY, the peak observed at 258 nm initially increased in intensity with 5 min of electrolysis indicating the formation of a product but with time the intensity of the band started to decrease simultaneously with an increment of a band at 268 nm. This could indicate that the initial product started to turn a new product. For AR, the peaks at 268 nm increases their intensity with 5 min of electrolysis, but then started to decrease accompanied with a bathochromic shift. Similarly to SY, the initial products change with electrolysis. Finally, for P4, a new band at 264 nm appears with electrolysis showing the presence of a new product. In all cases, the bands that increases in intensity are localized in the region associated to a π-π^* transition involving the aromatic rings and the bands associated to the azo-moiety decreased.

3.3. Electrooxidation pathway of colorants on glassy carbon electrode at neutral pH

The electrochemical measurements indicate that the oxidation of the azo-colorants here studied involved 1$\bar{e}$ for AR and P4, and 2$\bar{e}$ for SY. The evidence presented in this work suggests that these colorants share a common pathway for the loss of the first electron. The spectroelectrochemical results showed that the electrooxidation of the colorants produced the discoloration of the solutions, which was closely related to the disappearance of the bands commonly attributed to the azo bond. The nature of this band was confirmed after the identification of the azo orbitals as an important contribution to the molecular orbitals involved in the electronic transitions associated to that band. This result reveals that the loss of this band after the oxidation is related to impairment in the electronic and probably the structural integrity of the azo-moiety. Thereby, our experimental and theoretical results suggest that the oxidation occurs through the azo moiety, supported by the molecular orbital analysis, which identified the azo-moiety as the most active center towards oxidation processes; this because the HOMO orbital is mostly localized in the azo bond (orbital 105 for SY, 117 for AR and 138 for P4; Fig. 6 and Fig S-2). Therefore, we proposed that the oxidation pathway of the azo-colorants will give a radical cation centered in the azo-moiety, which is characterized by the resonance structures proposed in Scheme 2. This proposed radical cation and its resonance structures are supported by the quantification and localization of the spin density after the oxidation of the colorant. This computational method provides the most stable configuration of the unpaired electron in the molecule without bias, identified by the subtraction of the α-spin density and the β-spin density of the molecule. The results obtained (Fig. 8) are in complete agreement with the proposed pathway and is easy to identify that the unpaired electron is mainly localized in the azo-bond for all the colorants, with some delocalization in the aromatic rings, as expected from the proposed resonance structures. For SY, the radical also delocalized in the naphthol group next to the

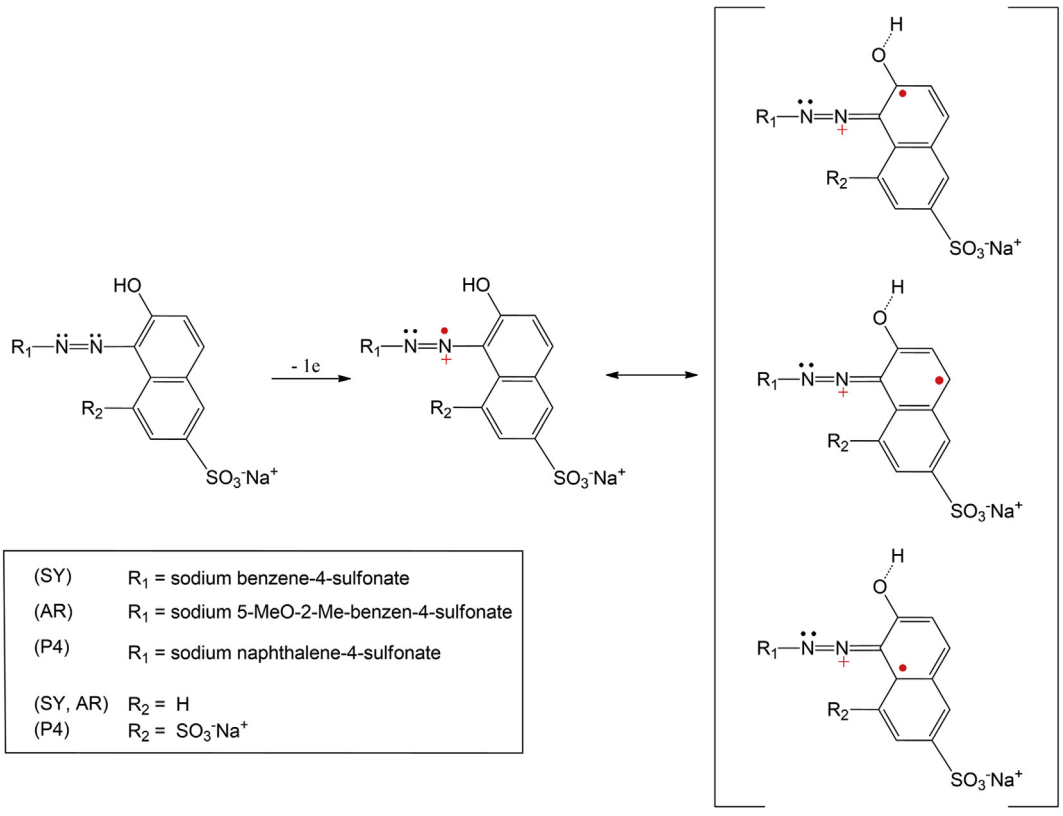

Scheme 2. Proposal pathway for the electrooxidation of azo colorants with the formation of a radical cation localized in the azo-moiety.

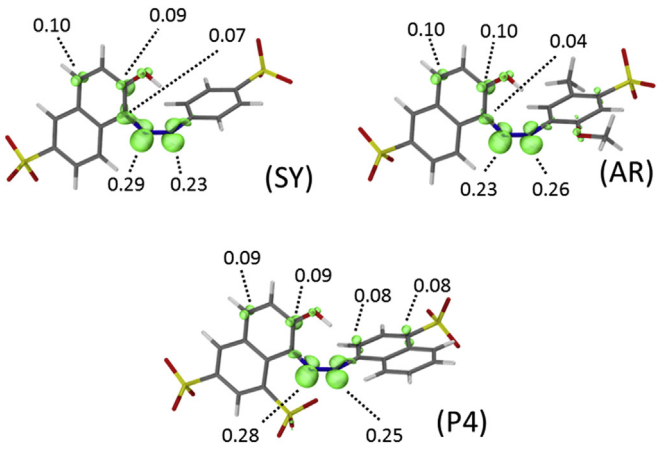

Fig. 8. Spin density obtained after the removal of 1ē of the colorants.

azo-moiety, but in a minor quantity, which is in agreement with the resonant structures proposed in Scheme 2. The same trend is observed for AR, the radical delocalized mostly in the azo bond and then in the naphthol group. In the case of SY and AR, both colorants have almost the same chemical structure but AR has more functional groups attached to the benzyl ring compare to SY. However, these groups did not affect the delocalization of the electron. In the case of P4, the azo bond connects a naphthol group with a naphthyl group; the delocalization of the electron in this molecule is mostly in the azo bond, and then is equally distributed between the naphthyl/naphthol groups. This result also corroborated the stability observed by spectroelectrochemical measurements for P4, which was the only colorant that did not completely discolor during the electrolysis.

4. Conclusions

Herein, we presented a characterization of the oxidation pathway for azo-colorants. For this purpose, we proposed an electrochemical approach complemented with spectroscopic and theoretical methods in order to obtain a complete representation of the process. Our approach allowed us to obtain new insights regarding the oxidation process of azo-colorants, pinpointing the azo group as the main oxidation center of the molecule. According to this, the subsequent steps should be related to the chemical modifications suffered by the azo moiety. The present work is the first stage of a complex study to determine the oxidation pathway of azo colorants focused into solving the redox center of the molecule, which was commonly assigned to the −OH group. Further progress in the characterization of the oxidation products is currently being made. Also, we are actively investigating the next steps involved in the oxidation process of a major group of colorants, which will be published soon. Finally, the methods combined in this work proved to be a powerful approach to provide a deeper understanding of the electrochemical processes with more chemical detail.

Acknowledgments

P.S-R thanks FONDECYT (Chile) for research grant No. 1170901. S.M-R thanks for the computational resources generously provided by the Department of Chemical Sciences, Universidad Andres Bello and to project DI-1323-16/R.

Appendix A. Supplementary data

Supplementary data to this article can be found online at https://doi.org/10.1016/j.electacta.2018.09.090.

References

[1] A.M. Grumezescu, A.M. Holban, Natural and Artificial Flavoring Agents and Food Dyes, Elsevier Science, 2017.
[2] E.M. Ungureanu, A.C. Razus, L. Birzan, M.S. Cretu, G.O. Buica, Electrochemical study of azo-azulene compounds, Electrochim. Acta 53 (2008) 7089–7099, https://doi.org/10.1016/j.electacta.2008.04.087.
[3] J.J. Gooding, R.G. Compton, C.M. Brennan, J.H. Atherton, The mechanism of the electro-reduction of some azo dyes, Electroanalysis 8 (1996) 4–8, https://doi.org/10.1002/elan.1140080604.
[4] S. Chanlon, L. Joly-Pottuz, M. Chatelut, O. Vittori, J.L. Cretier, Determination of carmoisine, allura red and ponceau 4R in sweets and soft drinks by differential pulse polarography, J. Food Compos. Anal. 18 (2005) 503–515, https://doi.org/10.1016/j.jfca.2004.05.005.
[5] K. Yamjala, M.S. Nainar, N.R. Ramisetti, Methods for the analysis of azo dyes employed in food industry - a review, Food Chem. 192 (2016) 813–824, https://doi.org/10.1016/j.foodchem.2015.07.085.
[6] A. Bafana, S.S. Devi, T. Chakrabarti, Azo dyes: past, present and the future, Environ. Rev. 19 (2011) 350–371, https://doi.org/10.1139/a11-018.
[7] K.T. Chung, The significance of azo-reduction in the mutagenesis and carcinogenesis of azo dyes, Mutat. Res. Genet. Toxicol. 114 (1983) 269–281, https://doi.org/10.1016/0165-1110(83)90035-0.
[8] X. Ye, Y. Du, D. Lu, C. Wang, Fabrication of β-cyclodextrin-coated poly (diallyldimethylammonium chloride)-functionalized graphene composite film modified glassy carbon-rotating disk electrode and its application for simultaneous electrochemical determination colorants of sunset yello, Anal. Chim. Acta 779 (2013) 22–34, https://doi.org/10.1016/j.aca.2013.03.061.
[9] T. Gan, J. Sun, Q. Wu, Q. Jing, S. Yu, Graphene decorated with nickel nanoparticles as a sensitive substrate for simultaneous determination of sunset yellow and tartrazine in food samples, Electroanalysis 25 (2013) 1505–1512, https://doi.org/10.1002/elan.201300008.
[10] L. Yu, M. Shi, X. Yue, L. Qu, Detection of allura red based on the composite of poly (diallyldimethylammonium chloride) functionalized graphene and nickel nanoparticles modified electrode, Sensor. Actuator. B Chem. 225 (2016) 398–404, https://doi.org/10.1016/j.snb.2015.11.061.
[11] T.W. Bentley, D.J. Richards, M.G. Hutchings, Electrochemical oxidative substitution and dimerisation of 1-arylazo-2-naphthols, leading to a new synthesis of some unsymmetrical diarylamines, Tetrahedron Lett. 27 (1986) 5261–5264, https://doi.org/10.1016/S0040-4039(00)85185-0.
[12] L. Labiadh, A. Barbucci, G. Cerisola, A. Gadri, S. Ammar, M. Panizza, Role of anode material on the electrochemical oxidation of methyl orange, J. Solid State Electrochem. 19 (2015) 3177–3183, https://doi.org/10.1007/s10008-015-2928-2.
[13] Y. Zhao, D.G. Truhlar, The M06 suite of density functionals for main group thermochemistry, thermochemical kinetics, noncovalent interactions, excited states, and transition elements: two new functionals and systematic testing of four M06-class functionals and 12 other functionals, Theor. Chem. Acc. 120 (2008) 215–241, https://doi.org/10.1007/s00214-007-0310-x.
[14] Y. Zhao, D.G. Truhlar, A new local density functional for main-group thermochemistry, transition metal bonding, thermochemical kinetics, and noncovalent interactions, J. Chem. Phys. 125 (2006), 194101, https://doi.org/10.1063/1.2370993.
[15] R. Peverati, D.G. Truhlar, Improving the accuracy of hybrid meta-GGA density functionals by range separation, J. Phys. Chem. Lett. 2 (2011) 2810–2817, https://doi.org/10.1021/jz201170d.
[16] R. Peverati, D.G. Truhlar, M11-L: a local density functional that provides improved accuracy for electronic structure calculations in chemistry and physics, J. Phys. Chem. Lett. 3 (2012) 117–124, https://doi.org/10.1021/jz201525m.
[17] A.D. Becke, A new mixing of Hartree–Fock and local density-functional theories, J. Chem. Phys. 98 (1993) 1372–1377, https://doi.org/10.1063/1.464304.
[18] J.P. Perdew, K. Burke, M. Ernzerhof, Generalized gradient approximation made simple, Phys. Rev. Lett. 77 (1996) 3865–3868, https://doi.org/10.1103/PhysRevLett.77.3865.
[19] C. Adamo, V. Barone, Toward reliable density functional methods without adjustable parameters: the PBE0 model, J. Chem. Phys. 110 (1999) 6158–6170, https://doi.org/10.1063/1.478522.
[20] Y. Zhang, W. Yang, Comment on "Generalized gradient approximation made simple", Phys. Rev. Lett. 80 (1998) 890, https://doi.org/10.1103/PhysRevLett.80.890.
[21] A.D. Becke, Density-functional exchange-energy approximation with correct asymptotic behavior, Phys. Rev. A. 38 (1988) 3098–3100, https://doi.org/10.1103/PhysRevA.38.3098.
[22] J. Perdew, Density-functional approximation for the correlation energy of the inhomogeneous electron gas, Phys. Rev. B 33 (1986) 8822–8824, https://doi.org/10.1103/PhysRevB.33.8822.
[23] A.D. Becke, Density-functional thermochemistry. III. The role of exact exchange, J. Chem. Phys. 98 (1993) 5648, https://doi.org/10.1063/1.464913.

[24] C. Lee, W. Yang, R.G. Parr, Development of the Colle-Salvetti correlation-energy formula into a functional of the electron density, Phys. Rev. B 37 (1988) 785.
[25] M.J. Frisch, J.A. Pople, J.S. Binkley, Self-consistent molecular orbital methods 25. Supplementary functions for Gaussian basis sets, J. Chem. Phys. 80 (1984) 3265–3269, https://doi.org/10.1063/1.447079.
[26] D.G. Truhlar, C.J. Cramer, A. Lewis, J.A. Bumpus, J. Chem. Educ. 81 (2004) 596–604. J. Chem. Educ. 84 (2007) 934.
[27] A.V. Marenich, C.J. Cramer, D.G. Truhlar, Universal solvation model based on solute electron density and on a continuum model of the solvent defined by the bulk dielectric constant and atomic surface tensions, J. Phys. Chem. B 113 (2009) 6378–6396, https://doi.org/10.1021/jp810292n.
[28] J.J. Guerard, J.S. Arey, Critical evaluation of implicit solvent models for predicting aqueous oxidation potentials of neutral organic compounds, J. Chem. Theor. Comput. 9 (2013) 5046–5058, https://doi.org/10.1021/ct4004433.
[29] M.J. Frisch, G.W. Trucks, H.B. Schlegel, G.E. Scuseria, M.A. Robb, J.R. Cheeseman, et al., Gaussian 09, Revision B.01, Gaussian 09, Revis. B.01, Gaussian, Inc., Wallingford CT, 2009.
[30] C. Zoski, Handbook of Electrochemistry, First, New Mexico, USA, 2007, https://doi.org/10.1016/B978-044451958-0.50027-6.
[31] D. Jacquemin, E.A. Perpète, G.E. Scuseria, I. Ciofini, C. Adamo, TD-DFT performance for the visible absorption spectra of organic Dyes: conventional versus long-range hybrids, J. Chem. Theor. Comput. 4 (2008) 123–135, https://doi.org/10.1021/ct700187z.
[32] R. Bauernschmitt, R. Ahlrichs, Treatment of electronic excitations within the adiabatic approximation of time dependent density functional theory, Chem. Phys. Lett. 256 (1996) 454–464. https://doi.org/10.1016/0009-2614(96)00440-X.
[33] M.E. Casida, C. Jamorski, K.C. Casida, D.R. Salahub, Molecular excitation energies to high-lying bound states from time-dependent density-functional response theory: characterization and correction of the time-dependent local density approximation ionization threshold, J. Chem. Phys. 108 (1998) 4439–4449, https://doi.org/10.1063/1.475855.
[34] E.D. Glendening, A.E. Reed, J.E. Carpenter, F. Weinhold, NBO Version 3.1, TCI, Univ. Wisconsin, Madison, 1998, p. 65.
[35] L. Tian, C. Feiwu, Multiwfn: a multifunctional wavefunction analyzer, J. Comput. Chem. 33 (2011) 580–592, https://doi.org/10.1002/jcc.22885.
[36] A.J. Bard, L.R. Faulkner, Electrochemical Methods: Fundamentals and Applications, Wiley, 2000.
[37] D. Pletcher, S.E. Group, R. Greff, R. Peat, Instrumental Methods in Electrochemistry, Ellis Horwood, 2001.
[38] R.S.G. Bontempelli, F. Magno, G.A. Mazzocchin, Linear sweep and cyclic voltammetry, Ann. Chim. 79 (1989) 103–216.
[39] M. Wang, Z. Chen, Y. Chen, C. Zhan, J. Zhao, New synthesis of self-assembly ionic liquid functionalized reduced graphene oxide–gold nanoparticle composites for electrochemical determination of Sudan I, J. Electroanal. Chem. 756 (2015) 49–55, https://doi.org/10.1016/j.jelechem.2015.08.007.
[40] M. Wang, Y. Sun, X. Yang, J. Zhao, Sensitive determination of Amaranth in drinks by highly dispersed CNT in graphene oxide "' water '" with the aid of small amounts of ionic liquid, Food Chem. 179 (2015) 318–324, https://doi.org/10.1016/j.foodchem.2015.01.143.
[41] A.E. Vikraman, D. Thomas, S.T. Cyriac, K.G. Kumar, Kinetic and thermodynamic approach in the development of a voltammetric sensor for sunset yellow, J. Electrochem. Soc. 161 (2014) B305–B311, https://doi.org/10.1149/2.0581414jes.
[42] M.-C. Tsai, P.-Y. Chen, Electrochemical detection of 2-naphthol at a glassy carbon electrode modified with tosflex film, Electroanalysis 19 (2007) 1315–1321, https://doi.org/10.1002/elan.200703857.
[43] M.S. Ureta-Zañartu, P. Bustos, C. Berrıos, M.C. Diez, M.L. Mora, C. Gutiérrez, Electrooxidation of 2,4-dichlorophenol and other polychlorinated phenols at a glassy carbon electrode, Electrochim. Acta 47 (2002) 2399–2406, https://doi.org/10.1016/S0013-4686(02)00043-9.
[44] V.C. Diculescu, J.A.P. Piedade, A.M. Oliveira-Brett, Electrochemical behaviour of 2,8-dihydroxyadenine at a glassy carbon electrode, Bioelectrochemistry 70 (2007) 141–146, https://doi.org/10.1016/j.bioelechem.2006.03.015.
[45] E.M. Garrido, A. Maria, O. Brett, Electrochemical oxidation of bentazon at a glassy carbon electrode Application to the determination of a commercial herbicide 46 (1998) 1131–1135.
[46] O. Corduneanu, P. Janeiro, A.M.O. Brett, On the electrochemical oxidation of resveratrol, Electroanalysis 18 (2006) 757–762, https://doi.org/10.1002/elan.200503469.
[47] C. Barrientos, P. Navarrete-Encina, J. Carbajo, J.A. Squella, New voltammetric method useful for water insoluble or weakly soluble compounds : application to p K a determination of hydroxyl coumarin derivatives, J. Solid State Electrochem. 22 (2018) 1423–1429, https://doi.org/10.1007/s10008-017-3750-9.
[48] C. Nie, J. Dong, P. Sun, C. Yan, H. Wu, B. Wang, An efficient strategy for full mineralization of an azo dye in wastewater: a synergistic combination of solar thermo- and electrochemistry plus photocatalysis, RSC Adv. 7 (2017) 36246–36255, https://doi.org/10.1039/C7RA05797K.
[49] I. Ahmad, S. Murtaza, S. Ahmed, Electrochemical and photovoltaic study of sunset yellow and tartrazine dyes, Monatshefte Fur Chemie 146 (2015) 1631–1640, https://doi.org/10.1007/s00706-015-1425-8.
[50] K. Bevziuk, A. Chebotarev, D. Snigur, Y. Bazel, M. Fizer, V. Sidey, Spectrophotometric and theoretical studies of the protonation of allura red AC and ponceau 4R, J. Mol. Struct. (2017), https://doi.org/10.1016/j.molstruc.2017.05.001.
[51] Y.S. Mok, J.O. Jo, J.C. Whitehead, Degradation of an azo dye Orange II using a gas phase dielectric barrier discharge reactor submerged in water, Chem. Eng. J. 142 (2008) 56–64, https://doi.org/10.1016/j.cej.2007.11.012.
[52] A. Wang, J. Qu, H. Liu, J. Ge, Degradation of azo dye Acid Red 14 in aqueous solution by electrokinetic and electrooxidation process, Chemosphere 55 (2004) 1189–1196, https://doi.org/10.1016/j.chemosphere.2004.01.024.
[53] C. Ramírez, A. Saldaña, B. Hernández, R. Acero, R. Guerra, S. Garcia-Segura, et al., Electrochemical oxidation of methyl orange azo dye at pilot flow plant using BDD technology, J. Ind. Eng. Chem. 19 (2013) 571–579, https://doi.org/10.1016/j.jiec.2012.09.010.
[54] L.E.V. Salgado, C. Vargas-Hernandez, Spectrophotometric determination of the pKa , isosbestic point and equation of absorbance vs . pH for a universal pH indicator, Am. J. Anal. Chem. (2014) 1290–1301.
[55] A.R. da Cunha, E.L. Duarte, M.T. Lamy, K. Coutinho, Protonation/deprotonation process of Emodin in aqueous solution and pKa determination: UV/Visible spectrophotometric titration and quantum/molecular mechanics calculations, Chem. Phys. 440 (2014) 69–79, https://doi.org/10.1016/j.chemphys.2014.06.009.
[56] Z. Sun, Y. Chen, Q. Ke, Y. Yang, J. Yuan, Photocatalytic degradation of cationic azo dye by TiO2/bentonite nanocomposite, J. Photochem. Photobiol. A Chem. 149 (2002) 169–174, https://doi.org/10.1016/S1010-6030(01)00649-9.
[57] J.B. Parsa, M. Rezaei, A.R. Soleymani, Electrochemical oxidation of an azo dye in aqueous media investigation of operational parameters and kinetics, J. Hazard Mater. 168 (2009) 997–1003, https://doi.org/10.1016/j.jhazmat.2009.02.134.